International Journal of Nanomedicine

Dovepress
open access to scientific and medical research

Open Access Full Text Article

ORIGINAL RESEARCH

Minocycline-Loaded Poly(α-Lipoic Acid)–Methylprednisolone Prodrug Nanoparticles for the Combined Anti-Inflammatory Treatment of Spinal Cord Injury

Feng Lin[1,2]
Yixuan Liu[2,3]
Wenqi Luo[1,2]
Shuhan Liu[4]
Yiming Wang[1,2]
Rui Gu[1]
Wanguo Liu[1]
Chunsheng Xiao[2,5]

[1]Department of Orthopaedic Surgery, China-Japan Union Hospital of Jilin University, Changchun, 130033, People's Republic of China; [2]Key Laboratory of Polymer Ecomaterials, Changchun Institute of Applied Chemistry, Chinese Academy of Sciences, Changchun, 130022, People's Republic of China; [3]School of Applied Chemistry and Engineering, University of Science and Technology of China, Hefei, 230026, People's Republic of China; [4]Department of Neurosurgery, The First Hospital of Jilin University, Changchun, 130021, People's Republic of China; [5]Jilin Biomedical Polymers Engineering Laboratory, Changchun, 130022, People's Republic of China

Purpose: Traumatic spinal cord injury (TSCI) induces a powerful inflammatory response that can significantly exacerbate the extent and severity of neural damage (termed as "secondary injury"). Thus, the suppression of inflammation is crucial for reducing neurological dysfunction following TSCI. However, the conventional anti-inflammatory drugs show limited efficacy because of poor penetration and release kinetics at the injury site. This study describes the design, synthesis, release kinetics, biosafety, and preclinical efficacy of minocycline (MC)-loaded poly(α-lipoic acid)–methylprednisolone (PαLA-MP) prodrug nanoparticles (NPs) for the combined anti-inflammatory treatment of TSCI.

Methods: NPs were produced by conjugating MP to PαLA and then loading MC. The NP structure was confirmed through ^{1}H nuclear magnetic resonance (^{1}H NMR), Fourier transform infrared spectroscopy, ultraviolet–visible absorption spectroscopy, gel permeation chromatography, dynamic light scattering, and transmission electron microscopy. Drug-loading content and efficacy were measured using high-performance liquid chromatography (HPLC) or ^{1}H NMR and release kinetics through HPLC. Biosafety was examined using the MTT assay, cell penetration efficiency using confocal microscopy, and flow cytometry using Cyanine5 (Cy5)-labeled MC-PαLA-MP NPs, effects on injury-induced pro-inflammatory cytokine release using enzyme-linked immunosorbent assays and immunofluorescence, and treatment efficacy by measuring motor recovery in a rat model of TSCI.

Results: The MC-PαLA-MP NPs exhibited high biocompatibility and released 81% MC and 54% MP within 24 h under TSCI-like conditions, effectively reducing 40% of pro-inflammatory cytokine release both in cultures and injured rat spinal cord tissues. Systemic injection increased the Basso, Beattie, Bresnahan score of TSCI rats from 2.33 ± 0.52 to 8.83 ± 1.83 in 8 weeks, providing effective neuroprotection and enhanced exercise recovery in the TSCI rats.

Conclusion: The MC-PαLA-MP NPs can mitigate secondary inflammation and preserve motor function following experimental TSCI, which suggests their potential for clinical application.

Keywords: anti-inflammation, motor recovery, nanomedicine, neuroprotection, spinal cord injury

Introduction

Among the numerous biochemical changes that occur following traumatic spinal cord injury (SCI; TSCI), the inflammatory response is one of the most important determinants of secondary pathophysiological changes and lasting neurological dysfunction. This secondary inflammatory response is induced by the activation of resident macrophages (microglia) at the injury site, which release pro-inflammatory cytokines that, in

Correspondence: Rui Gu; Wanguo Liu
Tel +8613804371075; +8618186881807
Fax +86431-89876939; +86431-89876921
Email gurui@jlu.edu.cn; liuwanguo6016@jlu.edu.cn

Received: 22 October 2021
Accepted: 22 December 2021
Published: 7 January 2022

turn, promote the invasion and activity of other immune cells.[1,2] Through these processes, acute inflammation activates a positive feedback loop that sustains the inflammatory response for several days to weeks, resulting in additional tissue damage within and outside the region of traumatic injury (termed as "secondary injury").[3,4]

Several potential treatments have been developed to protect the surrounding healthy spinal cord tissues from inflammatory damage following TSCI, such as therapeutic hypothermia; hyperbaric oxygen therapy; intrathecal injection of chondroitinase ABC; and intravenous application of glucocorticoids, riluzoles, gangliosides, calcium channel blockers, and nerve growth factors.[3,5–10] However, only methylprednisolone (MP) has demonstrated efficacy in clinical trials and thus has been approved for the treatment of patients with TSCI.[11] MP binds glucocorticoid receptors to prevent nuclear translocation of pro-inflammatory transcription factors, thereby inhibiting the production and release of pro-inflammatory signaling factors (cytokines and chemokines) and limiting membrane lipid peroxidation.[11,12] However, owing to low accumulation and retention in the spinal cord, high MP doses must be administered as pulse therapy, which may induce side effects such as sepsis, gastrointestinal bleeding, and thromboembolism.[11–14] Therefore, there is a pressing need for more effective delivery strategies to achieve better therapeutic efficacy against TSCI while minimizing the side effects.

Nanodrug delivery systems are a promising strategy for improving drug bioavailability and tissue distribution because of the enhanced permeability and retention effect of nanoparticles (NPs).[13,15,16] Moreover, the local destruction of the blood–spinal cord barrier (BSCB) promotes the targeting of NPs to the injury site following systemic administration.[17,18] Thus far, carboxymethyl chitosan/polyamidoamine dendrimer NPs, poly(lactic-*co*-glycolic acid) NPs, and poly(ethylene-oxide)-poly(phenylene-oxide)-poly(ethylene-oxide) copolymeric micelles have been used as delivery vehicles for MP and have achieved therapeutic effects in preclinical models.[19,20] Furthermore, glutathione-pegylated liposomes and NEP140-conjugated human serum albumin were used to target deliver MP to the injured spinal cord.[21,22] However, these NPs release MP passively, which may be extremely slow to effectively suppress the rapid inflammatory response and ensuing pathophysiological changes following TSCI.[3,15]

In the present study, we constructed minocycline (MC)-loaded poly(α-lipoic acid)-MP (PαLA-MP) prodrug NPs (MC-PαLA-MP NPs) for the combined mitigation of the inflammatory response following TSCI. First, PαLA-*graft*-poly(ethylene glycol) was synthesized and used to conjugate MP to form a polymeric prodrug, PαLA-MP. Then, MC—an effective drug for the treatment of SCI—was loaded into PαLA-MP to prepare MC-PαLA-MP NPs. Our results showed that these MC-PαLA-MP NPs can rapidly release MC and MP at the injury site to achieve a combined anti-inflammatory effect, leading to improved neuroprotective effect and thus resulting in reduced neurodegeneration and greater functional recovery following experimental TSCI in rat models.[23,24]

Materials and Methods

Materials

α-Lipoic acid (αLA) was purchased from Jilin Chinese Academy of Sciences—Yanshen Technology (Changchun, China); MP, MC, and MTT or 3-(4,5-dimethyl-thiazol -2-yl)-2,5-diphenyl tetrazolium bromide from Dalian Meilun Biological Technology (*Dalian*, China); poly(ethylene glycol) monomethyl ether (mPEG; polymer molecular weight = 2000 g/mol) and 4′,6-diamidino-2-phenylindole (DAPI) from Sigma-Aldrich LLC (Shanghai, China); and N-hydroxysuccinimide (NHS), 4-dimethylaminopyridine (DMAP), and 1-(3-(dimethylamino) propyl)-3-ethylcarbodiimide hydrochloride (EDC·HCl) from ALADDIN Biochemical Technology (Shanghai, China). Deuterated dimethyl sulfoxide (DMSO-d_6) was obtained from the Energy Chemical Biochemical Technology (Shanghai, China). Lipopolysaccharide (LPS), Dulbecco's Modified Eagle's Medium (DMEM), and fetal bovine serum (FBS) were purchased from ThermoFisher Scientific (Shanghai, China) and Cyanine5-amino (Cy5-NH_2) from Ruixi Biological Technology (Xi'an, China). Deionized water was prepared using a Milli-Q system (Millipore, Billerica, MA, USA). Other chemicals were purchased from Sinopharm Chemical Reagent (Shanghai, China). All chemicals and reagents were used as received.

^{1}H nuclear magnetic resonance (^{1}H NMR) spectra were recorded in DMSO-d_6 using the AV-300 NMR spectrometer (Bruker, Billerica, MA, USA). The Fourier transform infrared (FT-IR) spectra were acquired using the Bio-Rad Win-IR spectrometer (Bio-Rad, Hercules, CA, USA), and the ultraviolet–visible (UV–Vis) absorption spectra was acquired using the UV-Lambda 365 spectrophotometer (PerkinElmer, Waltham, MA, USA). Polymer molecular weight and polydispersity were determined using a gel

permeation chromatography (GPC) system equipped with a Waters 515 HPLC pump and Waters 2414 Refractive Index Detector (Waters, Milford, MA, USA). A mobile phase of *N,N*-dimethylformamide at a flow rate was 1 mL/min and temperature of 25°C was used for polymer analysis. Dynamic laser scattering (DLS) was performed using the Malvern ZEN3600 instrument (Malvern, Worcestershire, UK). The fluorescence intensity was measured using the Fluorescence Master System (Photon Technology International Inc., Birmingham, NJ, USA). For transmission electron microscopy (TEM), a JEOL JEM-1011 microscope (JOEL, Tokyo, Japan) was used at an accelerating voltage of 100 kV. High-performance liquid chromatography (HPLC) was performed using a Waters 1525 system (Waters, Milford, MA, USA) equipped with a reverse-phase column (Symmetry® C18). A mobile phase comprising *N,N*-dimethylformamide and 0.2 mol/L ammonium acetate buffer (6:4 v:v) was used to analyze MC release, whereas that comprising acetonitrile and deionized water (4:6 v:v) was used to analyze MP release from MC-PαLA-MP NPs. For both measures, the flow rate was 1 mL/min and the temperature was 25°C. Electrospray ionization (ESI) mass-spectrometry (MS) was performed using the Fourier transform mass spectrometer (Bruker APEX-IV, Billerica, MA, USA). Cytotoxicity was assessed using the MTT assay, and the cytokine levels were measured using the enzyme-linked immunosorbent assay (ELISA) with an absorbance microplate reader (Infinite M200, Tecan, Switzerland). The cellular uptake was monitored via confocal laser scanning microscopy (CLSM; Zeiss LSM780, Oberkochen, Germany) and flow cytometric analysis (FCA; BD FACSCeleta™, Franklin Lakes, NJ, USA).

Cell Lines and Animals

Primary astrocytes purified from the cortex of postnatal day 5 rats were purchased from Bioleaf Biotech (Shanghai, China) and cultured to the fifth passage for subsequent experiments. The BV2 microglia cell line was obtained from BNCC (Beijing, China). The pheochromocytoma 12 (PC12) cell line was obtained from the Basic Medical College of Jilin University, and the use of the cell line was approved by Ethics Committee of Jilin University. Sprague Dawley (SD) rats (strain: inbred, sex: female, average body weight: 220–250 g, and age: 7–8 weeks) were purchased from Liaoning Changsheng Biotechnology (Liaoning, China). All animal protocols were in accordance with the Guidelines for Care and Use of Laboratory Animals of Jilin University, and experiments were approved by the Animal Ethics Committee of Jilin University (approval No. SY202103013).

Synthesis of PαLA

PαLA was synthesized as described previously.[25,26] In brief, α-lipoic acid (1.03 g; 5 mmol) was added to a dry flask under nitrogen flow and stirred at 100°C for 2 h. The crude polymer product was dissolved in 20 mL of tetrahydrofuran and poured into 200 mL of cold ether. This process was repeated thrice to obtain a sticky white solid. Finally, PαLA was obtained through filtration and vacuum drying (0.73 g; yield: 70.9%).

Synthesis of PαLA-mPEG-MP and Cy5-Labeled PαLA-mPEG-MP

First, PαLA (0.62 g) was dissolved in 15 mL dimethyl sulfoxide (DMSO). MP (0.23 g; 0.60 mmol), EDC·HCl (229 mg; 1.20 mmol), and DMAP (36 mg; 0.30 mmol) were also dissolved in 15.0 mL DMSO and then mixed with PαLA and stirred for 24 h at room temperature. Subsequently, mPEG (1.20 g; 0.60 mmol) and EDC·HCl (229 mg) were added and the mixture stirred at room temperature for another 24 h. The reaction mixture was dialyzed against DMSO for 2 days and deionized water for another 2 days using a dialysis bag with a molecular weight cutoff (MWCO) of 3500 Da. The final product, PαLA-MP, was obtained as a white powder after lyophilization (1.51 g; yield: 73.7%).

Cy5-PαLA-MP was prepared following the same methods. PαLA-MP (100 mg; containing 0.41 mmol carboxyl groups), Cy5-NH_2 (0.48 mg; 20 μmol), EDC·HCl (19.1 mg; 100 μmol), and NHS (3 mg; 10 μmol) were dissolved in 5 mL DMSO. The mixture was stirred for 24 h in the dark and dialyzed against deionized water for another 24 h. The Cy5-PαLA-MP was obtained through lyophilization (yield: 69%).

Preparation of PαLA-MP NPs and MC-PαLA-MP NPs

The MC-PαLA-MP NPs were prepared as mentioned in this section. PαLA-MP (100 mg) was dissolved in 8 mL DMSO and then added drop-wise to 80 mL phosphate-buffered saline (PBS; pH 7.4) under gentle stirring. After 2 h, the DMSO was removed through dialysis (MWCO: 3500 Da) against deionized water for 12 h with water replacement

every 2 h. The PαLA-MP NPs were obtained after lyophilization. Cy5-PαLA-MP NPs were prepared using similar methods, and the fluorescence intensity was determined using a fluorescence spectrometer. For MC loading, PαLA-MP (100 mg) and MC (20 mg) were dissolved in 8 mL DMSO. Then, this mixture was added drop-wise to 80 mL PBS (pH 7.4) under gentle stirring in the dark. After 2 h, free MC and DMSO were removed through dialysis (MWCO: 3500 Da) against deionized water for 12 h with water replacement every 2 h. The MC-loaded NPs were obtained through lyophilization under darkness.

The drug-loading content (DLC) and drug-loading efficiency (DLE) of these compounds were determined using HPLC or ^{1}H NMR spectra and calculated according to the following formulas:

DLC (%) = (weight of loaded drugs/weight of MC-PαLA-MP NPs) × 100%

DLE (%) = (weight of loaded drugs/weight of feeding drugs) × 100%.

Cellular Uptake

The cellular uptake rate and intracellular distribution of NPs were determined using CLSM and FCA. For CLSM, BV2 and PC12 cells were seeded in 6-well plates at 1.0×10^5 cells/well and cultured at 37°C under a 5% CO_2 for 24 h. Then, 200 μg of Cy5-PαLA-MP NPs dissolved in 200 μL DMEM were added to the culture and incubated for 1, 2, or 4 h, as indicated. After washing thrice with PBS, the cells were fixed with 4% formaldehyde for 20 min, followed by three additional washings with PBS. Subsequently, the cell nuclei were stained via incubation in DAPI for 5 min. Cells were then observed via CLSM.

For FCA, BV2 and PC12 cells were seeded in 6-well plates at 1.0×10^5 cells/well and cultured at 37°C under a 5% CO_2 for 24 h. Then, 200 μg of Cy5-PαLA-MP NPs dissolved in 200 μL DMEM were added to the culture and incubated for 1, 2, or 4 h. Cells were then washed thrice with PBS, detached with trypsin, washed again with PBS, collected, and resuspended in 1 mL PBS. Signals from Cy5 were measured via FCA. Untreated cells were used as controls.

Cell Viability Assay

The biocompatibilities of PαLA-MP and MC-PαLA-MP NPs were determined in the cultures of primary astrocytes, BV2 cells, and PC12 cells using the MTT assay. In brief, cells were seeded in 96-well plates at 7000 cells/well and cultured for 24 h. The medium was then replaced with 200 μL DMEM containing PαLA-MP or MC- PαLA-MP NPs at concentrations ranging from 31.25 to 1000 μg/mL. After incubation for 24 h, 20 μL of MTT solution (5.0 mg/mL) was added, and the cells were incubated for another 4 h. Subsequently, the medium was carefully removed, and 150 μL DMSO added into each well. After shaking for 5 min, the absorbance value of each well was measured at 490 nm on the microplate reader.

Release of Pro-Inflammatory Cytokines

The release rates of pro-inflammatory cytokines from activated BV2 cells was evaluated using an ELISA kit. In brief, the cells were seeded in 6-well plates at 3×10^5 cells/well and then activated with 1 μg/mL LPS for another 24 h. The cell culture medium was then replaced with 2 mL DMEM containing MC, MP, MC + MP, PαLA-MP NPs, or MC-PαLA-MP NPs (at final MC and MP concentrations of 5 and 6.9 μg/mL, respectively). After 24 h, the supernatant was collected, and pro-inflammatory cytokine release was measured using ELISA.

Animal Model of TSCI

The rat model of TSCI was developed using the Allen method. In brief, a T10 segment laminectomy was performed under pentobarbital anesthesia to expose the thoracic spinal cord. The exposed dorsal surface was then damaged at the laminectomy site by dropping a 40 g rod from a height of 60 mm. Criteria for successful model preparation were as follows: the impact site exhibited hemorrhage and edema, hind limbs exhibited retractable flapping, tail exhibited spasmodic wagging, and animal developed sluggish paralysis.[27,28] After surgery, the muscle, fascia, and skin were closed in layers, and the external skin was disinfected with iodophor. The animals were resuscitated in an incubator and provided with adequate food and water. Penicillin (2×10^6 U/kg/day) was administered for 3 days to prevent infection, and the bladder was massaged twice daily until the bladder function was restored. A separate sham group also underwent laminectomy with no spinal impact.

Treatment of the TSCI Rats

Rats were randomly divided into eight groups comprising six rats each. An untreated sham group was used as the negative control. TSCI rats received intravenous injection of either 1) saline, 2) 10 mg/kg MC, 3) 14 mg/kg MP, 4) 10 mg/kg MC + 14 mg/kg MP, 5) 54 mg/kg PαLA-MP

NPs, 6) 32 mg/kg MC-PαLA-MP NPs, or 7) 64 mg/kg MC-PαLA-MP NPs within 5 min of injury.

Locomotor Assessment

The Basso, Beattie, Bresnahan (BBB) locomotor rating scale was used to evaluate the hind limb locomotor function following TSCI.[29] At 1 day and 1–8 weeks after injury, two independent researchers blinded to the treatment group rated the locomotor function according to the BBB criteria. The recovery time of the bladder function was also recorded during these assessments.

Histological Analysis and Immunohistochemistry

Rats were deeply anesthetized with pentobarbital sodium and perfused via the left ventricle with PBS and 4% paraformaldehyde. A 2-cm section of spinal cord was collected at the injury site and fixed with 4% paraformaldehyde. After dehydration in gradient ethanol, the tissue segment was embedded in paraffin and sectioned in the coronal plane. The sections were stained with hematoxylin and eosin (H&E) and Luxol fast blue (LFB, a myelin stain) and then were examined under an optical microscope.

The expression levels of tissue injury marker proteins and pro-inflammatory factors were estimated through immunofluorescence staining. In brief, paraffin sections were permeabilized with 0.1% Triton X-100 PBS for 15 min, blocked with 10% goat serum for 1 h, incubated with the indicated primary antibodies overnight at 4°C, and then incubated with appropriate secondary antibodies at room temperature for 2 h. The nuclei were counterstained through the immersion of the sections in DAPI for another 5 min. Finally, the sections were observed via CLSM. All images were acquired at the same exposure settings for comparison across the treatment groups.

In vivo Expression of Pro-Inflammatory Cytokines

The rats were deeply anesthetized and euthanized. After sacrifice, a 1-cm segment of injured spinal cord was collected and homogenized in precold PBS. The cell lysates were centrifuged at 12,000 × g for 20 min at 4°C, and the supernatants were retained. The total protein content in the lysate was measured using the Bicinchoninic Acid Protein Assay Kit. The levels of tumor necrosis factor (TNF)-α, interleukin (IL)-1β and IL-6 in the supernatant samples with equal amounts of protein were measured using ELISA.

Statistical Analysis

All results are presented as the mean ± SD. Treatment group means were compared via one-way analysis of variance using the GraphPad Prism Software (version 8.4.2; GraphPad Software Inc., San Diego, CA USA). *p < 0.05 (two-tailed) was considered significant for all tests.

Results and Discussion

Synthesis and Characterization of PαLA-MP

The synthesis of PαLA-MP is presented in Scheme 1. First, PαLA was synthesized by the ring-opening polymerization of αLA. The ^{1}H NMR spectra showed that the proton hydrogens adjacent to the sulfur atom were shifted right from 3.60 ppm and 3.15 ppm to 2.83 ppm, indicating the successful synthesis of PαLA (Figure S1, Supporting Information).[25,26] The UV−Vis spectrum of PαLA also showed that there was no characteristic peak of dithiolane at 330 nm, further confirming successful PαLA synthesis (Figure S2, Supporting Information).[30]

Next, MP and mPEG were conjugated to PαLA via esterification to obtain the PαLA-MP prodrug. The successful synthesis of PαLA-MP was confirmed using ^{1}H NMR, FT-IR, and GPC analyses. All expected peaks of PαLA, MP, and mPEG were detected in the ^{1}H NMR spectrum of PαLA-MP (Figure S1, Supporting Information). PαLA-MP also demonstrated high DLC for MP (17.7 wt%). Furthermore, the characteristic peak of carbonyl at 1734 cm^{-1} was found in the FT-IR spectrum, confirming the successful modifications of MP and mPEG (Figure S3, Supporting Information). In addition, the molecular weight was 95 kDa according to GPC analysis, which was consistent with the expected molecular weight of PαLA-MP (Figure S4, Supporting Information). In summary, all spectroscopic and GPC results confirmed the successful synthesis of PαLA-MP.

Preparation and Characterization of NPs

Owing to its amphiphilic property, PαLA-MP can self-assemble into NPs. As measured by DLS, the average hydrodynamic diameter of PαLA-MP was 81 nm, and the polydispersity index (PDI) was 0.326 (Figure S5A, Supporting Information). TEM revealed a uniform spherical morphology with an average diameter of

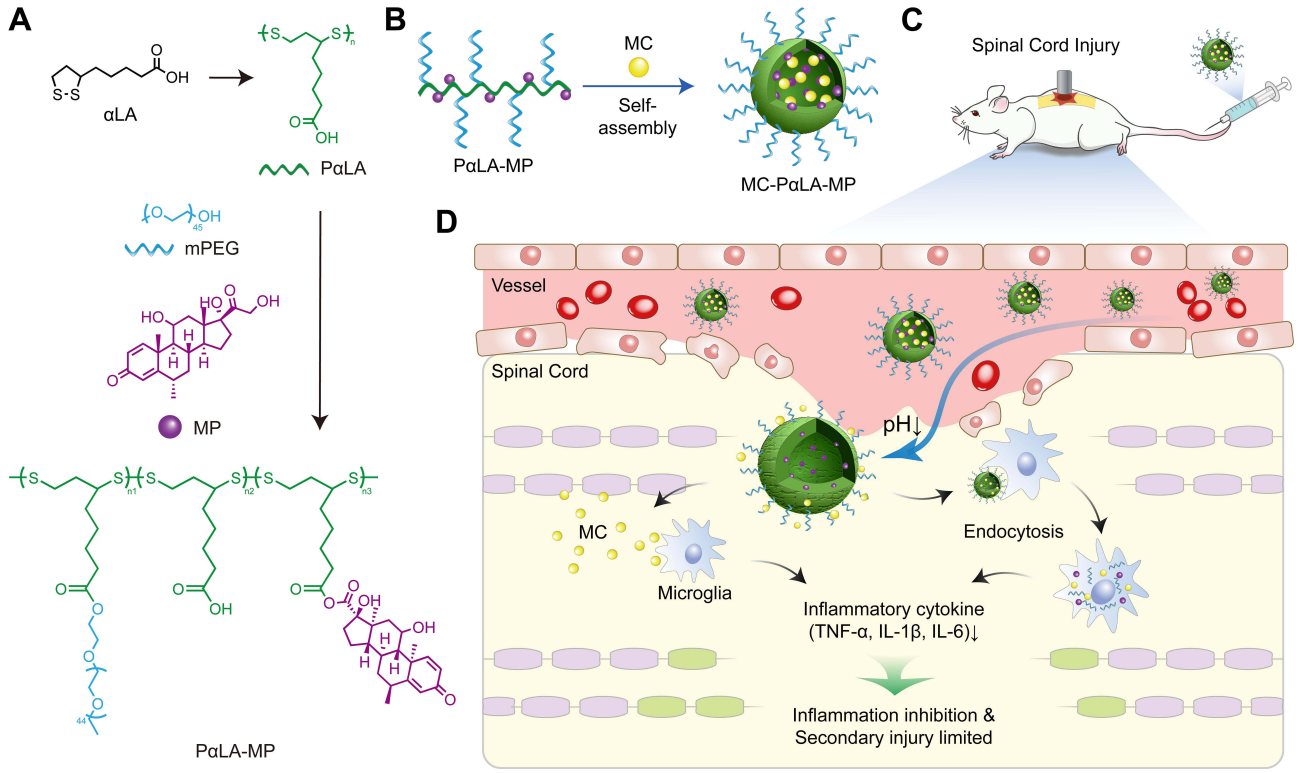

Scheme 1 Construction of minocycline (MC)-loaded poly(α-lipoic acid)–methylprednisolone (MP) prodrug nanoparticles (MC-PαLA-MP NPs). (**A**) Synthesis of PαLA-MP. (**B**) Self-assembly of MC-PαLA-MP NPs. (**C**) Intravenous injection of MC-PαLA-MP NPs to treat traumatic spinal cord injury (TSCI) rats. (**D**) Microenvironment-responsive drug release and the mechanism of phased inflammation inhibition after TSCI.

approximately 60 nm, slightly smaller than the size measured using DLS (Figure S5B, Supporting Information).

As an anionic polymer, PαLA can efficiently encapsulate positively charged drugs.[31,32] MC is a positively charged drug with a highly hydrophobic group and can be effectively encapsulated by PαLA-MP.[33] As expected, the encapsulation efficiency of MC by PαLA-MP NPs was high, as indicated by the DLC of 15.9 wt% and DLE of 79.5%. The high DLE of MC is likely attributable to the strong electrostatic interaction with PαLA-MP. Moreover, MC-PαLA-MP NPs exhibited an average hydrodynamic diameter of 121 nm, PDI of 0.10, and spherical shape averaging 79 nm in diameter (Figure 1A and B). Moreover, MC-PαLA-MP NPs were larger than PαLA-MP NPs, indicating the successful incorporation of MC.[26] The MC-PαLA-MP NP size was maintained for 3 days in PBS and PBS containing 10% FBS, indicating its excellent stability in the aqueous environment (Figure S6, Supporting Information).

In vitro Release of NPs

These MC-PαLA-MP NPs showed faster MC release at a weakly acidic pH (6.8) than at the physiological pH (7.4), reaching 81% of the total loaded MC within 24 h (Figure 1C). This high release rate at pH = 6.8 may be because of the increased protonation of the carboxyl groups in PαLA and concomitant weakening of the electrostatic interaction with MC. After incubation with esterase (220 U/mL) for 48 h,[23] nearly 54% of the total MP concentration used was also released within 24 h (Figure 1D). In contrast, there was no detectable release of MP in esterase-free aqueous medium.

We also performed ESI-MS analysis using the solution released from the esterase treatment group at 48 h. We found that MP exists in the form of pristine drugs in the released solution; thus, drugs may still have pharmacological effects after release (Figure S7, Supporting Information). These results suggest that MC-PαLA-MP NPs have the capacity for rapid MC release at the weakly acidic injury site and slower sustained release of MP catalyzed by extracellular esterases, thereby producing a stronger combined anti-inflammatory response.

Cellular Uptake of NPs

The primary therapeutic targets of MC and MP are likely intracellular; thus, the drug efficacy may depend on the

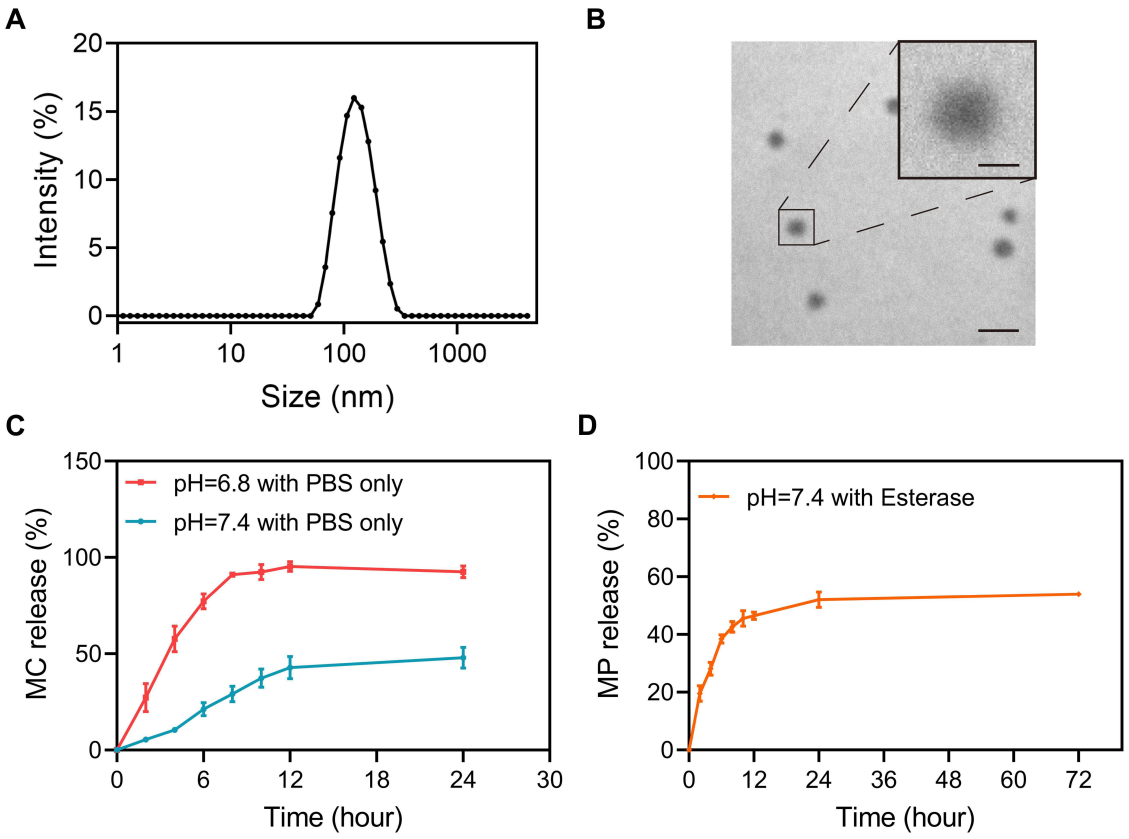

Figure 1 Physical characterization and in vitro release kinetics of MC-PαLA-MP NPs. (**A**) Dynamic light scattering (DLS) measurement of MC-PαLA-MP NP size distribution. (**B**) Transmission electron microscopy (TEM) image of MC-PαLA-MP NPs revealing a spherical shape of approximately 60 nm mean diameter. Scale bars are 200 and 50 nm, respectively (**C**) Minocycline (MC) release from MC-PαLA-MP NPs in the aqueous medium. (**D**) Methylprednisolone (MP) release from MC-PαLA-MP NPs in the aqueous medium.

efficiency of NP endocytosis. Therefore, cellular internalization was assessed in BV2 and PC12 cells via CLSM and FCA using Cy5-labelled PαLA-MP NPs.[34] Cy5-PαLA-MP NPs showed similar size and morphology compared with PαLA-MP NPs, and the successful loading of Cy5 was also confirmed using UV−Vis and fluorescence spectra (Figure S8, Supporting Information). Strong red fluorescent signals were observed in Cy5-PαLA-MP NP-treated BV2 cells, and the fluorescent intensity increased with incubation time (Figure 2A and C). In contrast, weaker fluorescence was detected in PC12 cells after the same incubation time (Figure 2B and D). Similar results were also noted after FCA (Figure 2E–H). Thus, PαLA-MP NPs may be effectively endocytosed by microglia but are less efficiently endocytosed by neurons.

In vitro Cytotoxicity

To evaluate the biosafety of PαLA-MP NPs and MC-PαLA-MP NPs, we first performed in vitro MTT cytotoxicity assays[35] using astrocytes, BV2 cells, and PC12 cells after exposure to 0–1000 μg/mL NPs for 24 h. Even at 1000 μg/mL, the mean cell viability was >90% in all cultures, suggesting that these NPs possess good biocompatibility and, thus, may be safe for the treatment of SCI (Figure 3A–C).

In vitro Anti-Inflammatory Effects of NPs

To characterize the anti-inflammatory effects of these NPs, the release rates of the pro-inflammatory cytokines IL-1β, IL-6, and TNF-α into the culture medium were measured in untreated control as well as LPS-activated and NP-treated LPS-activated BV2 cells using ELISA.[4,15,33] Compared with the resting control cells, LPS-activated cells showed markedly elevated levels of inflammatory cytokines. The treatment with MC-PαLA-MP NPs was roughly as effective as the combined MC–MP treatment (Figure 3D–F) in suppressing the release of IL-6 and TNF-α, although not in suppressing the release of IL-1β. This surprising in vitro efficacy of MC-PαLA-MP NPs may be because of sustained drug release (Figure 1) and efficient endocytosis (Figure 2). In contrast, PαLA-MP NPs demonstrated a poor anti-inflammatory effect, possibly because of the slow hydrolysis of MP in the absence of esterases.

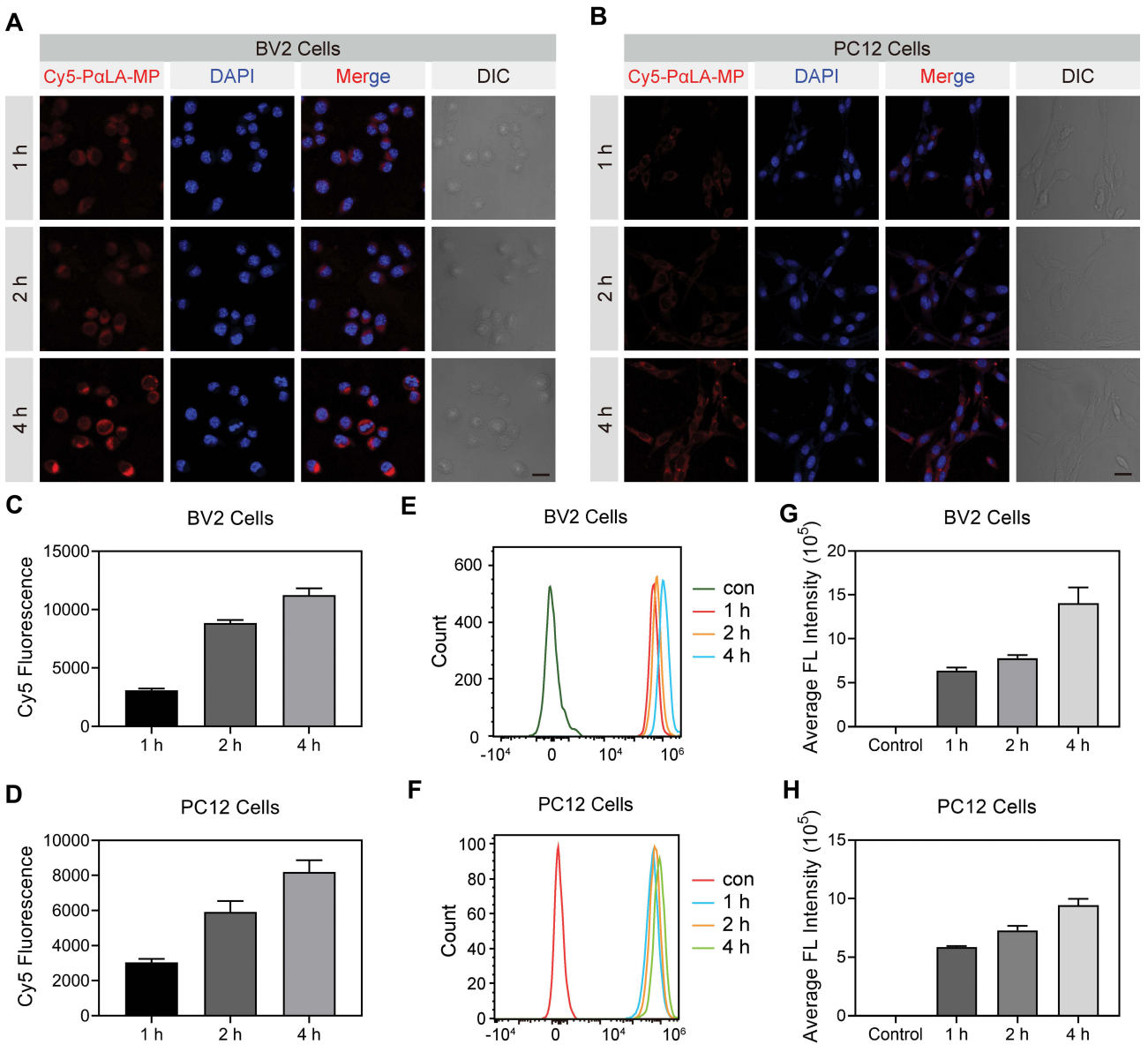

Figure 2 Cellular uptake efficiency of Cy5-labeled PαLA-MP NPs. (**A** and **B**) Confocal laser scanning microscopy (CLSM) images of (**A**) BV2 microglial and (**B**) PC12 cells after incubation with Cy5-PαLA-MP NPs for 1, 2, or 4 h. (**C** and **D**) Semiquantitative analysis of Cy5 fluorescence intensity in (**C**) BV2 and (**D**) PC12 cells from CLSM images. (**E** and **F**) Flow cytometry analysis (FCA) results of Cy5 uptake into (**E**) BV2 and (**F**) PC12 cells incubated with Cy5-PαLA-MP NPs for 1, 2, or 4 h. (**G** and **H**) Cy5 fluorescence intensity in (**G**) BV2 and (**H**) PC12 cells measured using semiquantitative FCA.

Therapeutic Effects of MC-PαLA-MP NPs in Rat Models of TSCI

To comprehensively evaluate the therapeutic efficacy of MC-PαLA-MP NPs in the rat model of TSCI, we first investigated the biodistribution of the Cy5-labeled PαLA-MP NPs after intravenous administration.[36] At 6 h after injection, a fluorescent signal was observed in the injured spinal cord that remained for at least 72 h (Figure S9, Supporting Information). This rapid accumulation might have been facilitated by the breach of the BSCB during TSCI. In contrast, the fluorescence intensity in other tissues decreased significantly after 24 h, indicating that PαLA-MP NPs can be effectively cleared from the body, thereby reducing the potential side effects.

Next, the therapeutic effects of MC-PαLA-MP NPs were investigated by periodically evaluating the BBB locomotor function for up to 8 weeks after TSCI.[37] Initially, the TSCI rats exhibited a complete loss of hind limb locomotion. Subsequently, differing degrees of functional restoration were observed in all treatment groups over the 2−5 weeks after injury, including a gradual increase in the weight-bearing

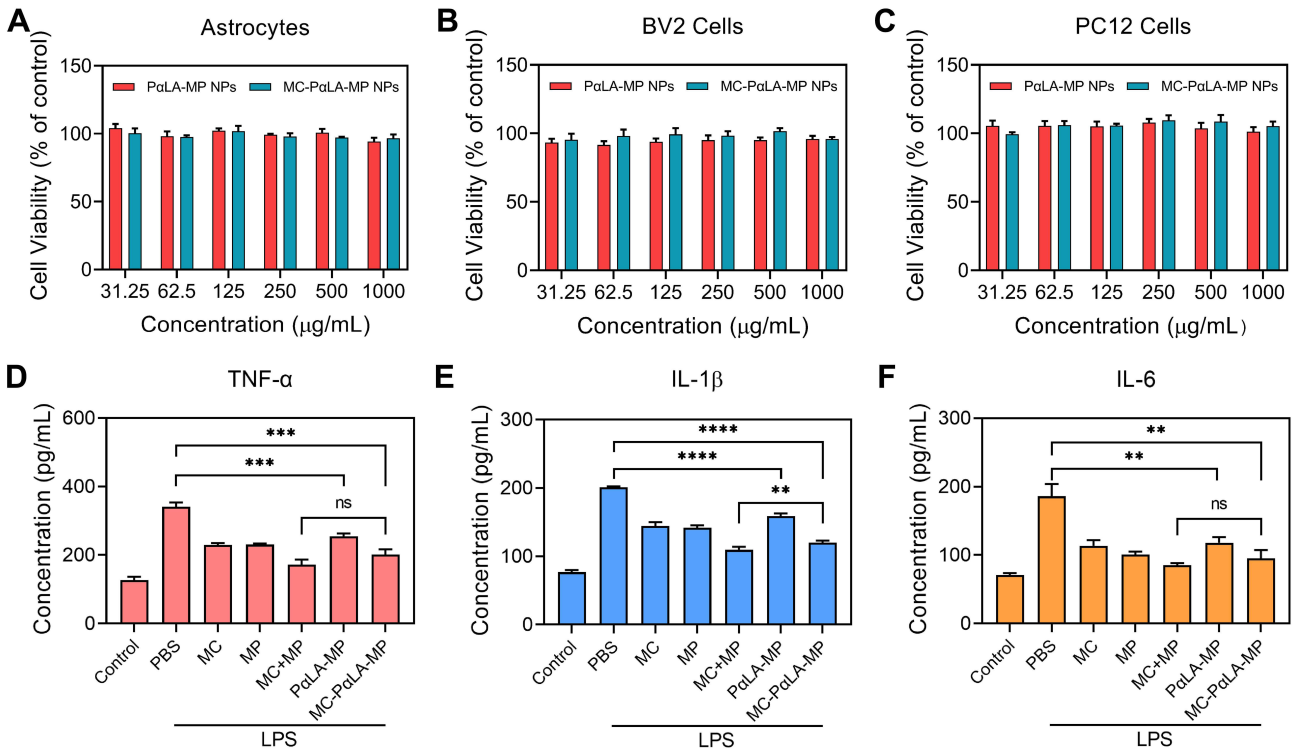

Figure 3 In vitro biocompatibility and anti-inflammatory efficacy of MC-PαLA-MP NPs. (**A**–**C**) Viabilities of (**A**) astrocytes, (**B**) BV2 microglial cells, and (**C**) PC12 cells after incubation with different concentrations of PαLA-MP NPs or MC-PαLA-MP NPs. (**D**–**F**) Release rates of (**D**) TNF-α, (**E**) IL-1β, and (**F**) IL-6 from lipopolysaccharide-activated BV2 cells treated with the vehicle (phosphate buffer saline), MC-PαLA-MP NPs, or various NP components. ****$p < 0.0001$; ***$p < 0.001$; **$p < 0.01$.
Abbreviation: ns, no significant difference.

ability of the lower limbs. These improvements are reflected by the gradual increase in the BBB scores (Figure 4A). Finally, all groups reached a functional recovery plateau at 6–8 weeks after injury. Compared with saline and PαLA-MP NP treatments, the high-dose MC-PαLA-MP (H-MC-PαLA-MP) treatment demonstrated the best therapeutic efficacy, as indicated by the highest BBB score (8.83 ± 1.83) at 8 weeks after injection (Figure 4A and B). The greater efficacy than the MC

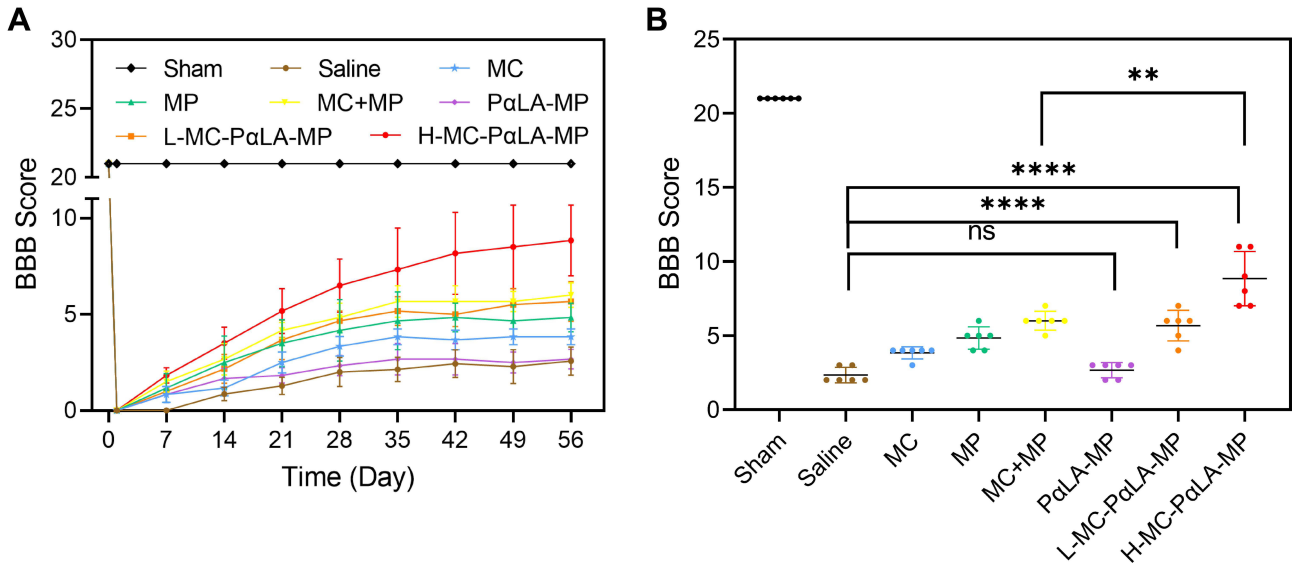

Figure 4 Facilitated recovery of the hind limb motor function by MC-PαLA-MP NPs. (**A**) Basso, Beattie, Bresnahan (BBB) scores of TSCI rats receiving the indicated treatments. (**B**) Final BBB scores at 8 weeks after injury. ****$p < 0.0001$; **$p < 0.01$.
Abbreviation: ns, no significant difference.

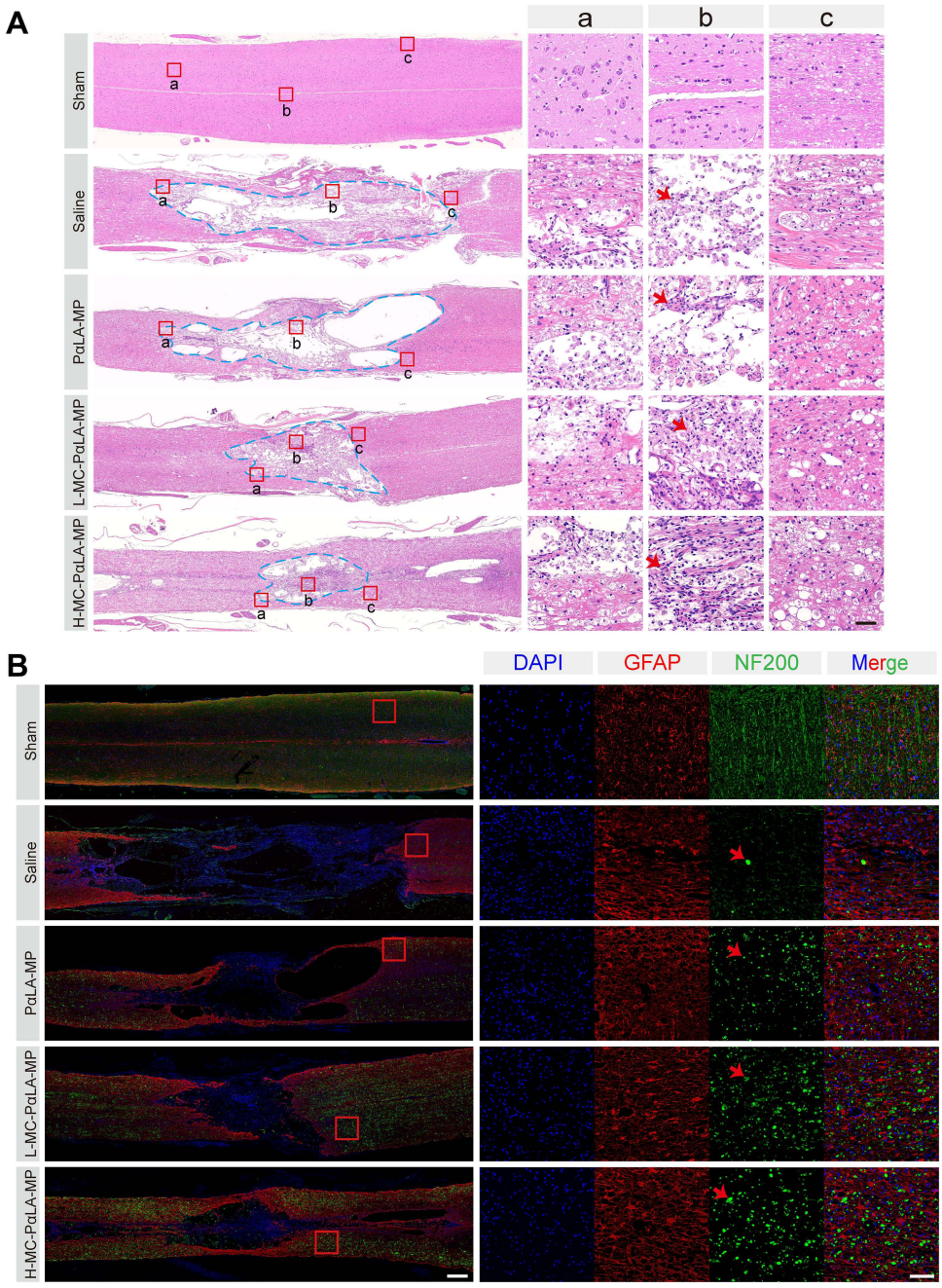

Figure 5 Histopathological changes induced by TSCI and mitigation by MC-PαLA-MP NPs. (**A**) Images of injured spinal cord stained with hematoxylin and eosin (H&E). Low magnification images are on the left (2×), and higher magnification images of the boxed regions are on the right (20×). Scale bars are 500 and 50 μm, respectively. (**B**) Immunofluorescence staining for the astrocyte marker glial fibrillary acid protein (red) and the neuronal marker NF200 (green) in the injured spinal cord. Low magnification images (2×) are on the left, and higher magnification images (10×) on the right. Scale bars are 500 and 100 μm, respectively. Arrows indicated the pathological characteristics.

+ MP treatment likely reflects the superior targeting and regulated release of MC and MP from the MC-PαLA-MP NPs at the injury site, leading to a greater mitigation of inflammation in both acute and chronic phases following TSCI.[3,33] In contrast, PαLA-MP NPs did not effectively promote functional recovery, possibly because of the slow release rate of MP and concomitant unchecked inflammation during the early phase following TSCI. Thus, MC-PαLA-MP NPs promote superior functional recovery through a dual anti-inflammatory effect mediated by the rapid MC release during the early phase and delayed but sustained MP release during the later phase following TSCI.

We also examined the effects on neurogenic bladder, a frequent complication of TSCI.[38,39] Consistent

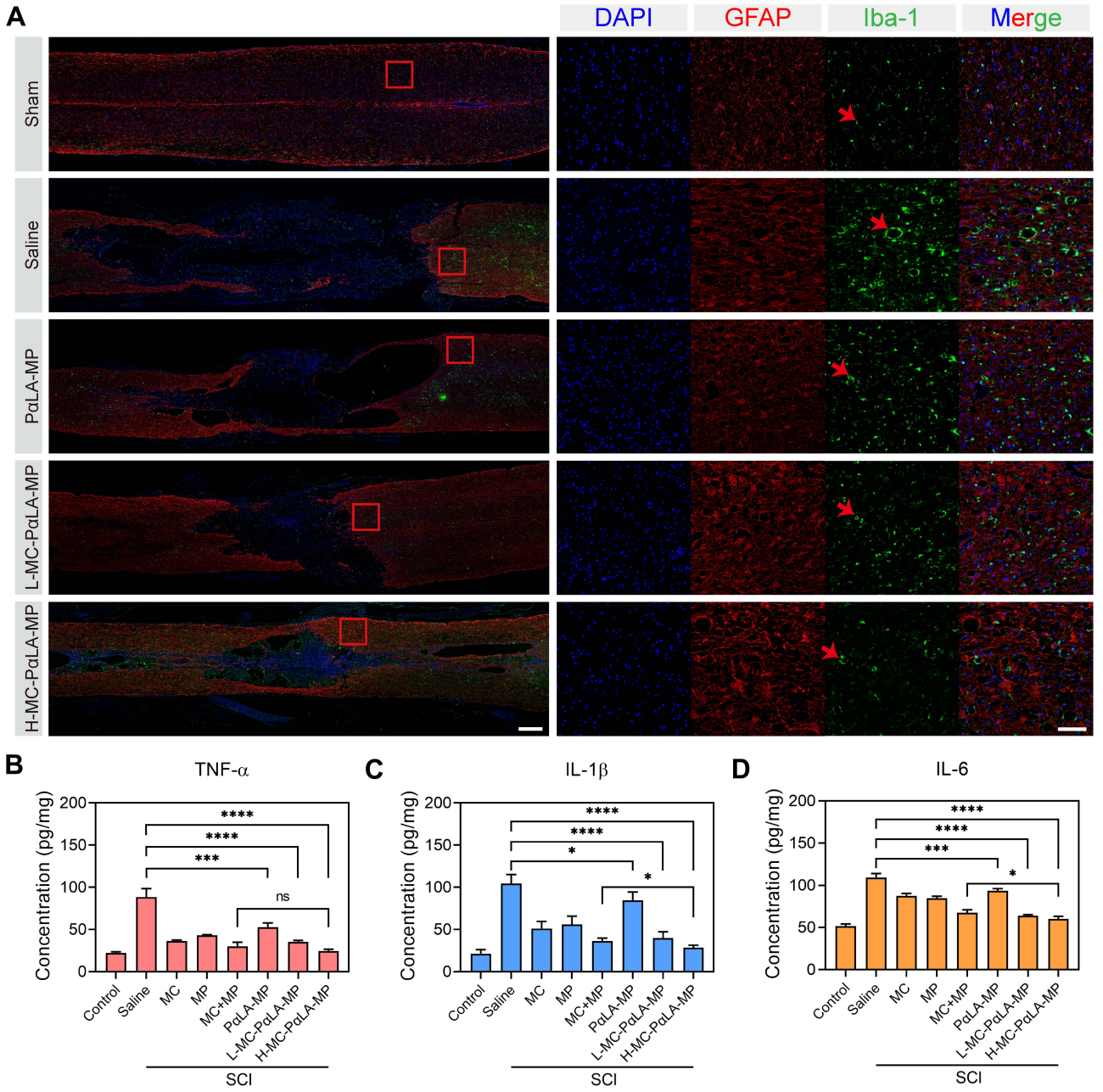

Figure 6 Treatment of TSCI rats with intravenous MC-PαLA-MP NPs significantly reduced microglial activation, astrocyte activation, and production of pro-inflammatory cytokines at the injury site. (**A**) Immunofluorescence images of activated astrocytes (glial fibrillary acid protein-positive, red) and microglia (Iba1-positive, green) in the injured spinal cord. Low magnification images (2×) are on the left, and higher magnification images (10×) of the outlined areas are on the right. Scale bars are 500 and 100 μm, respectively. Arrows indicated the pathological characteristics. (**B**–**D**) Immunoexpression of (**B**) TNF-α, (**C**) IL-6, and (**D**) IL-1β in the spinal cord of TSCI rats receiving the indicated treatments. ****$p < 0.0001$; ***$p < 0.001$; *$p < 0.05$.
Abbreviation: ns, no significant difference.

with motor recovery, MC-PαLA-MP NPs effectively inhibited the progression of neurogenic bladder, as evidenced by reduced bladder endometriosis and fibrosis compared with the other treatment groups (Figure S10, Supporting Information).

To investigate the physiological basis of locomotor recovery in the TSCI rats, changes in histopathological features were evaluated via H&E and immunofluorescence staining of spinal cord coronal sections at 8 weeks after injury.[37] In the saline group, a large number of apoptotic neurons were observed at the injury site and the continuity of the spinal cord was interrupted by large cavities (pan necrosis; Figures 5A, B, and S11, Supporting Information). In contrast, the

H-MC-PαLA-MP group showed significantly fewer apoptotic neurons and better tissue continuity than the other treatment groups, consistent with functional recovery measures.

We also evaluated the white matter integrity using LFB staining because progressive demyelination and associated impulse conduction impairment frequently lead to the sustained loss of function following SCI.[3,40,41] Consistent with functional recovery results, the H-MC-PαLA-MP group demonstrated the highest degree of myelin preservation (Figure S12, Supporting Information).

Anti-Inflammatory Effect of MC-PαLA-MP NPs in vivo

To further investigate the neuroprotective mechanisms of MC-PαLA-MP NPs, we performed immunofluorescence staining of reactive astrocytes and activated microglia because the densities of these cells are indicative of the neuroinflammation severity and potentially worse secondary injury. In the saline group, there were large numbers of glial fibrillary acid protein (GFAP) -positive reactive astrocytes and Iba-1-positive activated microglia as well as neuronophagy signs around the necrotic neurons—three hallmarks of severe neuroinflammation, whereas Iba-1 immunostaining intensity was markedly reduced in all other treatment groups (Figures 6A and S13, Supporting Information) with greatest reduction in the MC-PαLA-MP NP group.

Activated microglia in the injury site can release several inflammatory cytokines such as TNF-α, IL-1β, and IL-6, which amplify inflammation[3,40] and further aggravate SCI.[2] To investigate the mechanisms through which MC-PαLA-MP NPs preserve tissue integrity and promote functional recovery, we evaluated the inhibitory effect on inflammatory cytokine production using ELISA (Figure 6B–D).[40] As expected, the levels of TNF-α, IL-1β, and IL-6 were significantly elevated at the injury sites in all groups after TSCI compared with the sham group. The treatment with MC-PαLA-MP NPs reduced TNF-α, IL-1β, and IL-6 immunoreactivities to a greater extent than that all other treatments, including MC plus MP, consistent with functional and histopathological results. These findings strongly suggest that MC-PαLA-MP NP inhibits the progression of secondary SCI by reducing the release of inflammatory cytokines.

Biocompatibility of NPs

According to previous studies, high doses of MC or MP can cause significant systemic toxicity and even death.[11,42] Therefore, this study also examined potential tissue toxicity using H&E staining (Figure S14, Supporting Information). The analysis of stained sections revealed no significant differences in the histopathological signs of toxicity across the treatment groups, further confirming the safety and biocompatibility of MC-PαLA-MP NPs.

Conclusion

We developed MC-PαLA-MP NPs for the combined inhibition of neuroinflammation following TSCI. In vivo and in vitro studies confirmed that these MC-PαLA-MP NPs possess favorable drug release kinetics and biocompatibility and can effectively inhibit the generation of inflammatory reactions and improve the recovery of motor function after TSCI. Therefore, systemic MC-PαLA-MP NP administration is a promising strategy for the clinical treatment of spinal cord injury.

Acknowledgments

We acknowledge the financial support from the National Natural Science Foundation of China (51803072, 51773196, and 51573184), Jilin Provincial Science and Technology Program (20180520207JH, 20200201341JC), Jilin Provincial Finance Program (2019SCZ023, 2018SCZ013), and the Bethune Plan Research Project of Jilin University (2018B15 and 470110000648).

Disclosure

The authors report no conflicts of interest in this work.

References

1. McDonald JW, Sadowsky C. Spinal-cord injury. *Lancet*. 2002;359:417–425. doi:10.1016/S0140-6736(02)07603-1
2. Tran AP, Warren PM, Silver J. The biology of regeneration failure and success after spinal cord injury. *Physiol Rev*. 2018;98:881–917. doi:10.1152/physrev.00017.2017
3. Ahuja CS, Wilson JR, Nori S, et al. Traumatic spinal cord injury. *Nat Rev Dis Primers*. 2017;3:17018. doi:10.1038/nrdp.2017.18
4. Beattie MS. Inflammation and apoptosis: linked therapeutic targets in spinal cord injury. *Trends Mol Med*. 2004;10:580–583. doi:10.1016/j.molmed.2004.10.006
5. Fischer I, Dulin JN, Lane MA. Transplanting neural progenitor cells to restore connectivity after spinal cord injury. *Nature Rev Neurosci*. 2020;21(7):366–383. doi:10.1038/s41583-020-0314-2

6. Bradbury EJ, Carter LM. Manipulating the glial scar: chondroitinase ABC as a therapy for spinal cord injury. *Brain Res Bull*. 2011;84:306–316. doi:10.1016/j.brainresbull.2010.06.015
7. Feng JJ, Li YH. Effects of hyperbaric oxygen therapy on depression and anxiety in the patients with incomplete spinal cord injury (a STROBE-compliant article). *Medicine*. 2017;96. doi:10.1097/MD.0000000000007334
8. Yuan B, Pan S, Zhang WW. Effects of gangliosides on expressions of caspase-3 and NGF in rats with acute spinal cord injury. *Eur Rev Med Pharmacol*. 2017;21:5843–5849.
9. Kusuyama K. Upregulation of calcium channel alpha-2-delta-1 subunit in dorsal horn contributes to spinal cord injury-induced tactile allodynia. *Spine J*. 2018;18:1062–1069. doi:10.1016/j.spinee.2018.01.010
10. Martins BDC, Torres BB, de Oliveira KM, et al. Association of riluzole and dantrolene improves significant recovery after acute spinal cord injury in rats. *Spine J*. 2018;18:532–539. doi:10.1016/j.spinee.2017.10.067
11. Huang H, Young W, Skaper S, et al. Clinical neurorestorative therapeutic guidelines for spinal cord injury (IANR/CANR version 2019). *J Orthop Translat*. 2020;20:14–24. doi:10.1016/j.jot.2019.10.006
12. Xue M, Yong VW. Neuroinflammation in intracerebral haemorrhage: immunotherapies with potential for translation. *Lancet Neurol*. 2020;19:1023–1032. doi:10.1016/S1474-4422(20)30364-1
13. Bentley ER, Little SR. Local delivery strategies to restore immune homeostasis in the context of inflammation. *Adv Drug Deliv Rev*. 2021;178:113971. doi:10.1016/j.addr.2021.113971
14. Silva NA, Sousa N, Reis RL, Salgado AJ. From basics to clinical: a comprehensive review on spinal cord injury. *Prog Neurobiol*. 2014;114:25–57. doi:10.1016/j.pneurobio.2013.11.002
15. Song YH, Agrawal NK, Griffin JM, Schmidt CE. Recent advances in nanotherapeutic strategies for spinal cord injury repair. *Adv Drug Deliv Rev*. 2019;148:38–59. doi:10.1016/j.addr.2018.12.011
16. Dou Y, Li C, Li L, Guo J, Zhang J. Bioresponsive drug delivery systems for the treatment of inflammatory diseases. *J Control Release*. 2020;327:641–666. doi:10.1016/j.jconrel.2020.09.008
17. Boyd BJ, Galle A, Daglas M, Rosenfeld JV, Medcalf R. Traumatic brain injury opens blood–brain barrier to stealth liposomes via an enhanced permeability and retention (EPR)-like effect. *J Drug Target*. 2015;23:847–853. doi:10.3109/1061186X.2015.1034280
18. Figley SA, Khosravi R, Legasto JM, Tseng Y-F, Fehlings MG. Characterization of vascular disruption and blood–spinal cord barrier permeability following traumatic spinal cord injury. *J Neurotrauma*. 2013;31:541–552. doi:10.1089/neu.2013.3034
19. Cerqueira SR, Oliveira JM, Silva NA, et al. Microglia response and in vivo therapeutic potential of methylprednisolone-loaded dendrimer nanoparticles in spinal cord injury. *Small*. 2016;12:972. doi:10.1002/smll.201503492
20. Kim Y-T, Caldwell J-M, Bellamkonda RV. Nanoparticle-mediated local delivery of methylprednisolone after spinal cord injury. *Biomaterials*. 2009;30:2582–2590. doi:10.1016/j.biomaterials.2008.12.077
21. Lin Y, Li C, Li J, et al. NEP140-modified human serum albumin nanoparticles enhance the therapeutic effect of methylprednisolone against spinal cord injury. *J Nanobiotechnol*. 2019;17:12. doi:10.1186/s12951-019-0449-3
22. Gaillard PJ, Appeldoorn CC, Rip J, et al. Enhanced brain delivery of liposomal methylprednisolone improved therapeutic efficacy in a model of neuroinflammation. *J Control Release*. 2012;164:364–369. doi:10.1016/j.jconrel.2012.06.022
23. Wang J, Li D, Liang C, et al. Scar tissue-targeting polymer micelle for spinal cord injury treatment. *Small*. 2020;16:1906415. doi:10.1002/smll.201906415
24. Xi K, Gu Y, Tang J, et al. Author Correction: microenvironment-responsive immunoregulatory electrospun fibers for promoting nerve function recovery. *Nat Commun*. 2021;12:2882. doi:10.1038/s41467-021-23438-9
25. Liu Z, Tang Z, Zhang D, et al. A novel GSH responsive poly(alpha--lipoic acid) nanocarrier bonding with the honokiol-DMXAA conjugate for combination therapy. *Sci China Mater*. 2020;63:307–315. doi:10.1007/s40843-019-1183-0
26. Yang H, Shen W, Liu W, et al. PEGylated Poly(α-lipoic acid) loaded with doxorubicin as a pH and reduction dual responsive nanomedicine for breast cancer therapy. *Biomacromolecules*. 2018;19:4492–4503. doi:10.1021/acs.biomac.8b01394
27. Young W. *In Progress in Brain Research*. Vol. 137. McKerracher L, Doucet G, Rossignol S, editors. Elsevier; 2002:231–255.
28. Liu W, Gu R, Zhu Q, et al. Rapid fluorescence imaging of spinal cord following epidural administration of a nerve-highlighting fluorophore. *Theranostics*. 2017;7:1863–1874. doi:10.7150/thno.18962
29. Basso DM, Beattie MS, Bresnahan JC. A sensitive and reliable locomotor rating scale for open field testing in rats. *J Neurotrauma*. 1995;12:1–21. doi:10.1089/neu.1995.12.1
30. Zhong Y, Zhang J, Cheng R, et al. Reversibly crosslinked hyaluronic acid nanoparticles for active targeting and intelligent delivery of doxorubicin to drug resistant CD44+ human breast tumor xenografts. *J Control Release*. 2015;205:144–154. doi:10.1016/j.jconrel.2015.01.012
31. Li Y, Yang H, Yao J, et al. Glutathione-triggered dual release of doxorubicin and camptothecin for highly efficient synergistic anticancer therapy. *Colloids Surf B Biointerfaces*. 2018;169:273–279. doi:10.1016/j.colsurfb.2018.05.025
32. Zhang P, Zhang Y, Ding X, et al. A multistage cooperative nanoplatform enables intracellular co-delivery of proteins and chemotherapeutics for cancer therapy. *Adv Mater*. 2020;32:2000013. doi:10.1002/adma.202000013
33. Wang X-J, Peng CH, Zhang S, et al. Polysialic-acid-based micelles promote neural regeneration in spinal cord injury therapy. *Nano Lett*. 2019;19:829–838. doi:10.1021/acs.nanolett.8b04020
34. Shen W, Liu W, Yang H, et al. A glutathione-responsive sulfur dioxide polymer prodrug as a nanocarrier for combating drug-resistance in cancer chemotherapy. *Biomaterials*. 2018;178:706–719. doi:10.1016/j.biomaterials.2018.02.011
35. Luo W, Wang Y, Lin F, et al. Selenium-doped carbon quantum dots efficiently ameliorate secondary spinal cord injury via scavenging reactive oxygen species. *Int J Nanomedicine*. 2020;15:10113–10125. doi:10.2147/IJN.S282985
36. Gao Y, Vijayaraghavalu S, Stees M, Kwon BK, Labhasetwar V. Evaluating accessibility of intravenously administered nanoparticles at the lesion site in rat and pig contusion models of spinal cord injury. *J Control Release*. 2019;302:160–168. doi:10.1016/j.jconrel.2019.03.026
37. Kim J-W Mahapatra C, Hong JY, et al. Functional recovery of contused spinal cord in rat with the injection of optimal-dosed cerium oxide nanoparticles. *Adv Sci*. 2017;4:1700034. doi:10.1002/advs.201700034
38. Wyndaele -J-J. The management of neurogenic lower urinary tract dysfunction after spinal cord injury. *Nat Rev Urol*. 2016;13:705–714. doi:10.1038/nrurol.2016.206
39. Zhang Y, Li L, Mu J, et al. Implantation of a functional TEMPO-hydrogel induces recovery from rat spinal cord transection through promoting nerve regeneration and protecting bladder tissue. *Biomater Sci*. 2020;8:1695–1701. doi:10.1039/C9BM01530B
40. Zhang T, Lin F, Liu W, et al. Reactive oxide species-scavenging lipid-polymer nanoparticles for neuroprotection after spinal cord injury. *Appl Mater Today*. 2021;24:101109. doi:10.1016/j.apmt.2021.101109
41. Saab AS, Nave K-A. A mechanism for myelin injury. *Nature*. 2016;529:474–475. doi:10.1038/nature16865
42. Wang Z, Nong J, Shultz RB, et al. Local delivery of minocycline from metal ion-assisted self-assembled complexes promotes neuroprotection and functional recovery after spinal cord injury. *Biomaterials*. 2017;112:62–71. doi:10.1016/j.biomaterials.2016.10.002